https://doi.org/10.5194/egusphere-2026-3602
Preprint. Discussion started: 9 July 2026

Isotope-Based Age Scale with Multi-Month Precision for the SE-Dome II Ice Core from Southeast Greenland Over the Past 150 Years

Saaya Hamamoto[1], Yoshinori Iizuka[2], Takuro Aizawa[3], Kaoru Kawakami[1,4], Mai Matsumoto[2], Sumito Matoba[2], Hayoung Bong[5,6], Kei Yoshimura[5,7], Atsushi Okazaki[8], Laura J. Dietrich[9], Hans Christian Steen-Larsen[9], Ryu Uemura[1*]

[1]Graduate School of Environmental Studies, Nagoya University, Nagoya, Japan
[2]Institute of Low Temperature Science, Hokkaido University, Sapporo, Japan
[3]National Institute of Polar Research, Tokyo, Japan
[4]Tokyo Metropolitan Research Institute for Environmental Protection, Tokyo Environmental Public Service Corporation, Tokyo, Japan
[5]Institute of Industrial Science, The University of Tokyo, Tokyo, Japan
[6]NASA Postdoctoral Program Fellow, NASA Goddard Institute for Space Studies, New York, United States
[7]Atmosphere and Ocean Research Institute, The University of Tokyo, Tokyo, Japan
[8]Institute of Advanced Academic Research, Chiba University, Chiba, Japan
[9]Geophysical Institute, University of Bergen and Bjerknes Center for Climate Research, Bergen, Norway

Correspondence to: Ryu Uemura (ryu.uemura@nagoya-u.jp)

Abstract

Precise age scales are essential for reconstructing past climate variability at high temporal resolution. Here, we present a new oxygen-isotope record for the SE-Dome II ice core from southeast Greenland and construct a multi-month-resolution age scale spanning 1871–2020 CE. The chronology, named SE2025iso, was developed by aligning oxygen-isotope variations in the ice core with isotope-enabled climate-model simulations. High snow accumulation at the SE-Dome site preserved multi-month variations of oxygen isotopes, allowing age determination beyond seasonal extremes. Although absolute validation at the monthly scale is challenging, the chronology has an estimated mean uncertainty of 2.0 months and is supported by multiple consistency evaluations, including melt and tritium horizons, seasonal accumulation comparisons, and also volcanic reference layers. The reconstructed snow accumulation rates correlate well with climate reanalysis data, except in summer. The reconstructed accumulation record shows that the weak seasonality at SE-Dome persisted throughout the past 150 years. This persistence suggests that the balance near the boundary between summer- and winter-dominated accumulation regimes across Greenland remained broadly stable despite recent Arctic warming. Applying the SE2025iso age scale to chemical records shows that hydrogen peroxide concentrations peak approximately 2–3 weeks after the summer solstice and that volcanic sulfate records exhibit reproducible post-eruption peaks at multi-month resolution. Overall, the SE2025iso chronology highlights the potential of high-accumulation ice-core sites for investigating multi-month-scale climate variability and aerosol deposition processes.

https://doi.org/10.5194/egusphere-2026-3602
Preprint. Discussion started: 9 July 2026

1 Introduction

A precise age scale is crucial for reconstructing paleoclimate records from ice cores. Ice core age scales are typically established, in intervals where seasonal layers are sufficiently resolvable, by identifying annual layer boundaries using multiple proxies such as ion concentrations (e.g., Na^+, Ca^{2+}, SO_4^{2-}, NO_3^-, NH_4^+) (Andersen et al., 2006), visual stratigraphy of dust layers (Alley et al., 1997), and electrical conductivity measurements (Hammer et al., 1994). Automated annual layer counting methods (Winstrup et al., 2012) have been introduced to objectively identify the annual layer boundary (Sinnl et al., 2022; Zhang et al., 2022). Although some studies on Greenland ice cores have successfully distinguished winter and summer seasons (Vinther et al., 2010) or assigned month-level ages by assuming accumulation rate scenarios in a year (Gfeller et al., 2014; Pasteris et al., 2014), resolving sub-annual to multi-month variability remains difficult. Such high-resolution dating is important for identifying characteristic peak months of aerosol and chemical species, which provide constraints on their emission, transport, and deposition processes. A key difficulty is that post-depositional processes, including vertical diffusion, mixing, and surface redistribution, smooth monthly to intra-annual proxy variations (Ollivier et al., 2025b).

In recent years, continuous flow analysis (CFA) techniques have enabled measurements of chemical species and water isotopes at sub-seasonal sampling resolution in polar ice cores. These developments have provided new opportunities to investigate seasonal variability and its long-term changes (Hughes et al., 2020; Jones et al., 2023; Vance et al., 2024). However, even with such high analytical resolution, the effective temporal resolution preserved in ice cores is often limited by diffusive smoothing. The attenuated isotope signal of seasonal variability needs to be reconstructed using a back-diffusion approach, and the potential uncertainties of such reconstructions have subsequently been discussed (Laepple et al., 2025; Jones et al., 2023). These studies mainly focus on reconstructing seasonal amplitude and its climatic interpretation, whereas resolving shorter, multi-month variability and establishing multiple chronological tie points within a single year remain challenging.

A high-resolution chronology for the SE-Dome I ice core in Greenland was constructed using an oxygen-isotope-based pattern-matching method (Furukawa et al., 2017). The SE-Dome I ice core (hereafter SE1 core) was retrieved from a high-accumulation site (1.02 m w.e. yr^{-1}) in southeast Greenland (Iizuka et al., 2016). This site likely experiences limited isotopic modification after snow deposition on the ice sheet because the high accumulation rate reduces both diffusion-related smoothing and precipitation intermittency. These conditions are advantageous for preserving continuous, high-resolution isotopic records, enabling the identification of proxy variability on a multi-month scale. The SE1 core age scale (SE-Dome Isotope age scale; hereafter, SEIS2016 age scale) was constructed by aligning oxygen isotope ratio ($\delta^{18}O$) variations in the ice core with those simulated by isotope-incorporated general circulation models and covers the period from 1958 to 2015 CE. This high-resolution age scale enabled the reconstruction of seasonal aerosol variations (Iizuka et al., 2018; Hattori et al., 2021). However, the SE1 $\delta^{18}O$ record is limited to this interval, and the reproducibility of its multi-month variability remains unverified. In addition, the potential influence of vapor–ice isotopic exchange, which depends on the strength of the vapor

https://doi.org/10.5194/egusphere-2026-3602
Preprint. Discussion started: 9 July 2026

flux (Dietrich et al., 2023), should be evaluated for the SE-Dome site, where relatively warm conditions may enhance vapor fluxes.

Resolving age at a multi-month scale provides advantages for paleoclimate studies. First, sub-annual dating precision allows for assessing snow accumulation rate variability on seasonal scales, essential for evaluating climate reanalysis data and model simulations at fine temporal and spatial scales. Second, it allows for a more detailed analysis of the seasonal cycle of chemical species, such as hydrogen peroxide (H_2O_2) (Neftel et al., 1984), whose production rate is influenced by solar radiation and atmospheric oxidation processes (Frey et al., 2005; Sakugawa et al., 2002). Previous studies have suggested that the timing of H_2O_2 peaks in ice cores may not always align with expected seasonal maxima due to post-depositional effects (Gfeller et al., 2014). Third, improved age resolution enhances the interpretation of volcanic eruption signals recorded in ice cores by distinguishing short-term depositional events from background sulfate variations. Such a high-resolution sulfate record will help to refine our understanding of stratospheric aerosol transport and deposition mechanisms following significant eruptions.

Here, we present a new $\delta^{18}O$ record from the 250.79 m-long SE-Dome II ice core (hereafter SE2 core) drilled at SE-Dome, Greenland, and develop a multi-month-resolution age scale covering the past 150 years. Unlike existing Greenland chronologies based mainly on annual-layer counting or volcanic synchronization, our age scale (SE2 2025 isotope age; hereafter, SE2025iso age) uses reproducible multi-month $\delta^{18}O$ structure constrained by isotope-enabled climate simulations. This approach does not replace established Greenland annual chronologies, but provides a complementary age model for a high-accumulation site where intra-annual isotope variability is unusually well preserved. For years prior to 1980 CE, we constructed the age scale using the $\delta^{18}O$ variations simulated from the historical reanalysis dataset 20CRv2 (Compo et al., 2011). We then evaluated the preservation of multi-month $\delta^{18}O$ variability, reconstructed the seasonal accumulation regime at the SE-Dome site, and illustrated the utility of the age scale through applications to H_2O_2 concentrations and volcanic sulfate signals. The methods are described in Sect. 2, and the results and discussion are presented in Sect. 3.

2 Materials and Methods

2.1 Ice Core Sample and Isotopic Measurement

The 250.79 m-long SE2 ice core was drilled at the SE-Dome (67°11'30"N, 36°28'12" W, 3161 m a.s.l.) in Greenland in 2021 (Iizuka et al., 2021) (Fig. 1). This new core extends the 90.45 m-long SE1 ice core (Iizuka et al., 2016). The SE-Dome is located at the apex of a domed topography with a high snow accumulation (1.02 m w.e. yr^{-1}), and the distance between SE1 and SE2 is ca. 5 km (Furukawa et al., 2017; Iizuka et al., 2021; Iizuka et al., 2016).

https://doi.org/10.5194/egusphere-2026-3602
Preprint. Discussion started: 9 July 2026

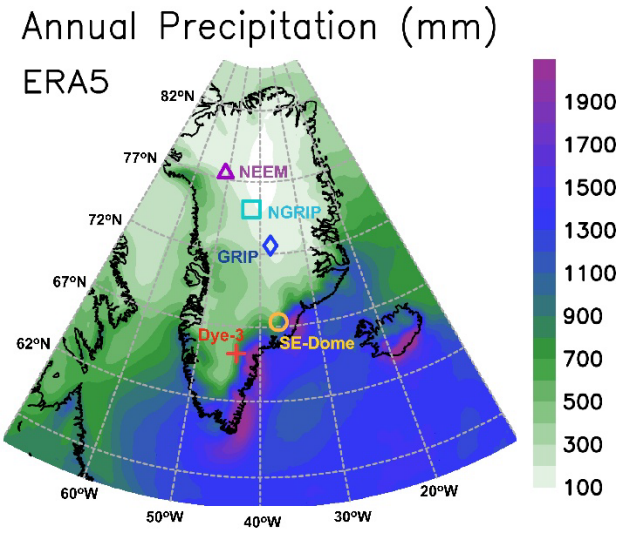

Figure 1. Locations of Greenland ice cores discussed in this study. Color shading shows annual mean precipitation over 1979-2014 CE from ERA5 reanalysis (Hersbach et al., 2020).

For isotope analysis, the SE2 core was cut into 4968 segments, each 5 cm in length, and stored in 20 mL glass bottles with plastic screw caps and rubber septa. The ice core samples were transported, frozen in glass bottles, and thawed before measurement. The $\delta^{18}O$ values were analyzed using cavity ring-down spectroscopy (L2130-i, Picarro Inc.). For each analysis, 375 µL of each sample was aliquoted into autosampler vials. For each measurement, an autosampler injected 1.8 µL of liquid water into the vaporizer (A0211, Picarro Inc.). The stable isotope ratio of oxygen ($\delta^{18}O$) is expressed as $\delta^{18}O = (R_{sample}/R_{VSMOW} - 1)$, where R_{sample} and R_{VSMOW} are the $^{18}O/^{16}O$ ratios of the sample and Vienna Standard Mean Ocean Water (VSMOW), respectively. Two laboratory standards were used to normalize $\delta^{18}O$ to the VSMOW-SLAP scale (Gonfiantini, 1978). The memory effect (analytical carryover between successive injections) was corrected (Gupta et al., 2009). Analytical reproducibility was evaluated by repeated measurements of GL21 working standard water ($\delta^{18}O$: −27.07‰) in each batch. The standard deviation (1σ) of GL21 over the measurement period (Dec. 2021–Oct. 2022) was ±0.04‰ (n = 83).

2.2 General Circulation Models with Isotopes

As targets for $\delta^{18}O$ pattern matching, we used isotope-incorporated general circulation models (GCMs), namely IsoGSM (Yoshimura, 2015; Yoshimura et al., 2008) incorporating global spectral nudging (Yoshimura and Kanamitsu, 2008), and MIROC5-iso (Okazaki and Yoshimura, 2017). The latest version, IsoGSM3 (Bong et al., 2024), which is nudged by ERA5, NCEP-R2, and JRA55, has a horizontal grid (ca. 200 km, T62), and its higher-resolution version, IsoGSM4 (ca. 50 km, T248), uses 28 vertical layers up to 10 hPa (ca. 30 km altitude), and a 6-hour output interval. The spatial resolution of

https://doi.org/10.5194/egusphere-2026-3602
Preprint. Discussion started: 9 July 2026

MIROC5-iso was set to T42 with 40 vertical layers (Okazaki and Yoshimura, 2017). Monthly $\delta^{18}O$ data for the grid containing the SE2 core drilling site were obtained by averaging the 6-hourly values weighted by precipitation amount.

To align the $\delta^{18}O$ pattern with that of the ice core, we used different isotope-incorporated GCMs based on the temporal resolution of the ice core and the availability of reanalysis datasets. First, since the shallow section of the ice core (2018–2020 CE) has higher resolution, a 2-weekly averaged dataset of IsoGSM4 nudged by ERA5 (Hersbach et al., 2020) was used. Second, for the dating 1980–2017 CE, monthly-averaged data from the isotope-enabled model dataset (Bong et al., 2024), including the average of IsoGSM3 and MIROC5-iso (JRA55), were used to match the ice core $\delta^{18}O$ pattern. The correlation between monthly $\delta^{18}O$ values across the GCMs exceeds $r = 0.70$, indicating high consistency among the models. Following Furukawa et al. (2017), we calculated the normalized isotope anomaly ($\delta^{18}O_{nor}$) defined as $(\delta^{18}O_{raw} - \delta^{18}O_{ave}) / \sigma_{18O}$, where $\delta^{18}O_{raw}$, $\delta^{18}O_{ave}$, σ_{18O} refer to the raw $\delta^{18}O$ value, its mean, and standard deviation, respectively. The multi-model mean $\delta^{18}O_{nor}$ was then used to align the ice-core $\delta^{18}O$ record for chronology construction. Finally, for periods not covered by climate reanalysis data (i.e., between 1871 CE and 1979 CE), IsoGSM nudged by the Twentieth Century Reanalysis data Version 2 (20CRv2; Compo et al., 2011) was used (Yoshimura and Kanamitsu, 2013; Yoshimura, 2015) (hereafter, IsoGSM20c run). The 20CRv2 assimilates surface pressure since 1871, with sea surface temperature and sea ice as boundary conditions.

2.3 Development of the Isotope-Based SE2 Age Scale 'SE2025iso'

The SE2 age scale was constructed using $\delta^{18}O$ pattern matching, following the method developed for the SE1 age scale (Furukawa et al., 2017). The $\delta^{18}O$ of the GCMs ($\delta^{18}O_{model}$) and the $\delta^{18}O$ of the SE2 ice core ($\delta^{18}O_{ice}$) were visually aligned to months and depths using intra-annual peaks and characteristic variations as tie points, establishing the preliminary depth–date relationship. To reduce errors of visual matching, we refined the age scale by three checks. First, three team members (S. H., R. U., and R. F.) independently performed $\delta^{18}O$ pattern matching using Analyseries Software (Paillard et al., 1996). Discrepancies were reviewed and attributed mainly to minor alignment offsets during manual tie-point selection, and final tie points were selected after reviewing discrepancies across the three independent matches. Second, we checked for inconsistencies using hydrogen peroxide (H_2O_2) seasonality, using the H_2O_2 dataset of Kawakami et al. (2023). In Greenland ice cores, H_2O_2 concentrations typically peak in July and reach a minimum in January (Gfeller et al., 2014). Tie points were revised only when H_2O_2 maxima or minima deviated by more than three months from these expected periods. These deviations were found in 14 sections, each representing a short core interval (typically 50 cm to 1 m) in which the offset persisted until the following winter minimum. This adjustment was used only to identify sections with implausible seasonal offsets and did not force H_2O_2 peaks to match July or any prescribed date. Third, we examined accumulation rates for anomalies. Anomalous accumulation rates exceeding four standard deviations (4σ) were flagged for review. Four sections were identified as outliers and were corrected by shifting the tie points to the adjacent multi-month cycle peak (one cycle earlier or later), thereby removing anomalous accumulation values. Finally, the SE2025iso age scale was derived by linear interpolation between the tie points.

https://doi.org/10.5194/egusphere-2026-3602
Preprint. Discussion started: 9 July 2026

2.4 Assessment of Post-Depositional Effects on Isotope Record

To estimate the impact of both diffusion and post-depositional processes at the SE-Dome, we used version 2.3 of the isotope-enabled surface-exchange and snowpack model SNOWISO (Wahl et al., 2022; Dietrich et al., 2023). Based on inputs of precipitation, sublimation, deposition, and isotopes in both precipitation and vapor, SNOWISO simulates one-dimensional profiles of the isotopic composition ($\delta^{18}O$, δD) in the snowpack. The model includes the impact of surface vapor-exchange-induced fractionation, which changes the isotopic composition of the surface snow post-depositionally, and applies it to the uppermost surface cell. In addition, snowpack diffusion (Johnsen, 2000) was applied to all cells at each timestep. The simulation has a vertical resolution of 2 cm and a temporal resolution of 30 minutes. The input data are based on a 30 × 30 km simulation with the regional climate model MAR (Dietrich et al., 2024), forced by ERA-5. The MAR latent heat fluxes were corrected based on observations from the accumulation zone of the Greenland Ice Sheet (Dietrich et al., 2024). Precipitation and isotopes were taken from an ECHAM6-wiso simulation (Cauquoin and Werner, 2021), forced by ERA-5. To match the observed accumulation at SE-Dome, we scaled the modeled precipitation input by a constant factor of 1.209, derived from the slope of the linear regression between observed annual accumulation and modeled precipitation over 1991–2019.

2.5 Reconstruction of Snow Accumulation

By constructing an age scale, accumulation rates can be independently determined from the depth–age relationship. Using the SE2025iso age scale, we determined annual and seasonal snow accumulation rates from 1872 to 2019. First, ice layer thicknesses were converted to water-equivalent thicknesses using high-resolution (1 mm) density data (Kawakami et al., 2023). Missing density values were interpolated linearly based on the averages of 1 cm above and below the gaps, and the interpolated data were averaged at 1 cm intervals. Second, the water-equivalent thicknesses of specific time intervals represent the snow accumulated during each period. However, ice at greater depths also experiences horizontal flow, leading to the thinning of the layers. Therefore, in the final step, accumulation rates were corrected for ice thinning caused by horizontal ice flow using the Nye model (Nye, 1963), assuming an ice sheet thickness of 1000 m at the SE2 site.

2.6 Detection of Volcanic Signals

To assess consistency with volcanic reference layers, we compared SE2 volcanic signals with those in the NEEM ice core (Sigl et al., 2013). Volcanic eruptions produce elevated sulfur concentrations in ice cores. These signals typically peak approximately one year after an eruption and serve as chronological markers. Volcanic sulfate deposition was identified when the annual mean sulfate concentration exceeded a threshold. Following Traufetter et al. (2004), the volcanic signal detection threshold is calculated as follows:

$$y_r = RM_i + kMAD_i \quad (1)$$

https://doi.org/10.5194/egusphere-2026-3602
Preprint. Discussion started: 9 July 2026

where y_r is the running threshold value, RM is the running median window of sample i, k is the threshold parameter, and MAD is the median of absolute deviation, representing background sulfate concentration. Following previous studies, we used k = 3 (Sigl et al., 2013) and set the window width to 21 years to reduce edge effects due to the short data period. We used the annual mean non-sea-salt sulfate (nss-SO_4^{2-}) concentrations of the SE2 core (Iizuka et al., 2025).

3 Results and Discussion

3.1 The SE2025iso Age Scale

3.1.1 Isotope Record and Construction of the Age Scale

The $\delta^{18}O$ profile of the SE2 core is shown in Fig. 2. The $\delta^{18}O$ values range from −35.5 to −16.6‰, with a mean of −27.5‰ and a standard deviation of 2.91‰. The data exhibit a recurring annual pattern, with a characteristic wavelength of approximately 1 m, corresponding to the annual accumulation rate. However, unlike a simple sinusoidal seasonal cycle, the SE2 record reveals distinct sub-annual $\delta^{18}O$ variations on a multi-month scale, with 20–40 cm variations. These finer-scale variations suggest that additional meteorological factors beyond the seasonal cycle influence $\delta^{18}O$ variability.

The SE2025iso age scale was constructed by aligning $\delta^{18}O$ variations in the ice core with those in isotope-incorporated GCM simulations (see Sect. 2.3), establishing a depth–age relationship for 1871–2020 CE (Fig. 2). The modeled and observed $\delta^{18}O$ variations show a strong correlation (r = 0.70) based on 722 tie points. Notably, in years where the winter minimum is less distinct (e.g., 2010, 2005, 1996, 1960, 1938, and 1917 CE), the model reproduces this feature in the ice-core record, reducing the risk of accidental annual-layer misidentification (e.g., failing to identify winter minima and mistakenly counting two years as one). Note that the automated annual-layer counting algorithm (Winstrup et al., 2012) yielded several-year offsets likely because of the pronounced 2–3-month intra-annual peaks of the SE2 core record (see Sect. 3.2.2).

Multi-month (approximately 2–3 months) $\delta^{18}O$ variations are consistently observed throughout the SE2 record. Although no strict periodicity is observed, a minor minimum frequently appears in spring, summer, and autumn. This pattern is generally reproduced in the model (e.g., 2013, 2002, 1990, and 1941 CE), indicating that these multi-month fluctuations likely reflect meteorological variability. Although their amplitude appears slightly dampened before 1900 CE, the multi-month structure remains identifiable down to 1871 CE.

https://doi.org/10.5194/egusphere-2026-3602
Preprint. Discussion started: 9 July 2026

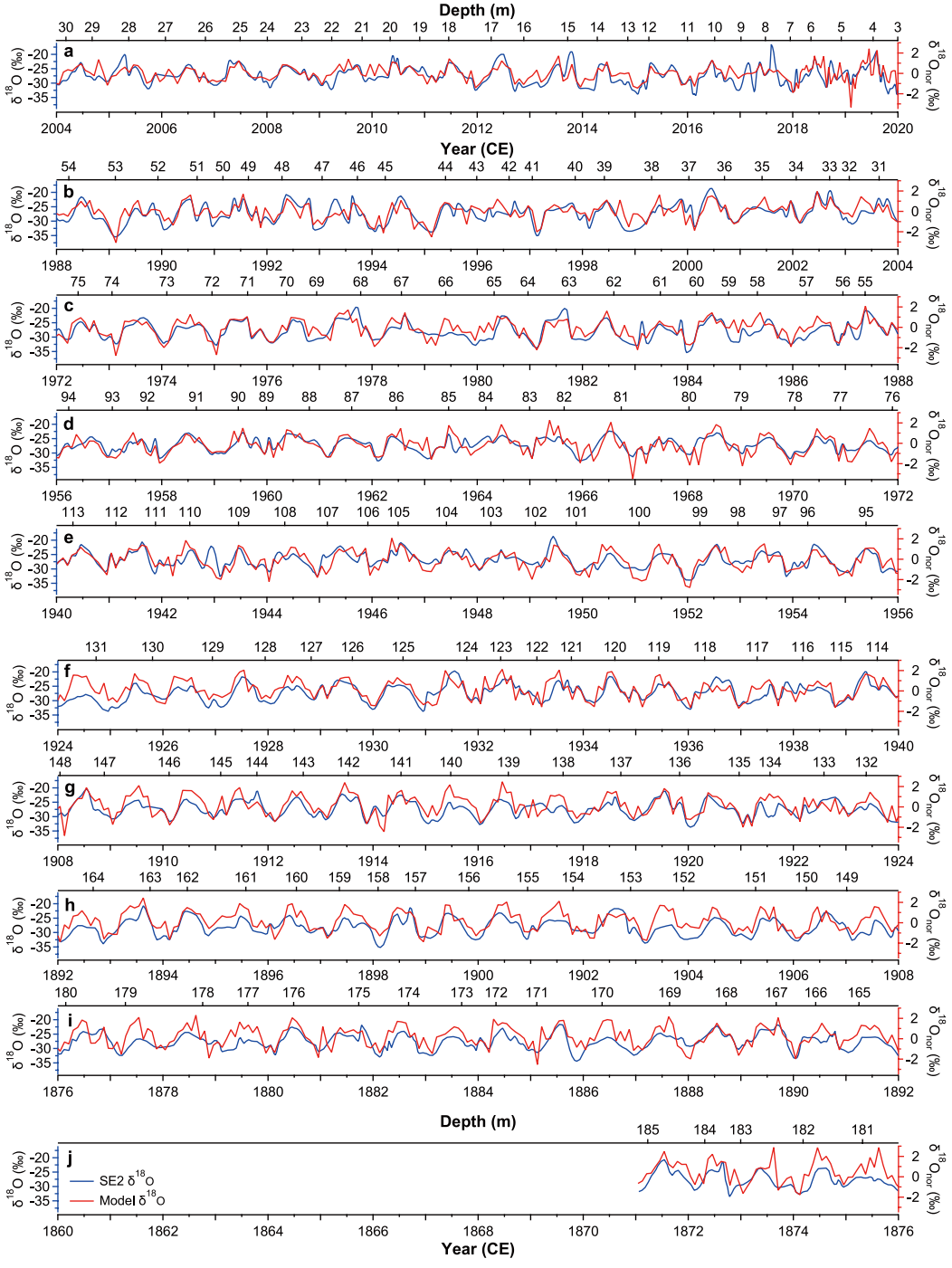

Figure 2. δ¹⁸O variations in the SE2 ice core and model simulations (1871–2020 CE). δ¹⁸O variations in the SE2 ice core (blue) and model simulations (red). The bottom X-axis shows the calendar year (CE), with the corresponding ice core depth (m) indicated at the top. For clarity, each panel covers 16 years.

https://doi.org/10.5194/egusphere-2026-3602
Preprint. Discussion started: 9 July 2026

3.1.2 Model–Data Comparison and Age Uncertainty

To assess the influence of temporal changes in model quality on the $\delta^{18}O$ pattern-matching approach, we evaluated the correlation between monthly $\delta^{18}O$ values from the SE2 ice core and those simulated by isotope-enabled GCMs using a 97-month running window (Fig. 3a). The correlation remains statistically significant ($p < 0.01$ for $r > 0.24$) throughout 1874–2013 CE, with r values generally exceeding 0.6. This correlation indicates that the model–data agreement is sufficiently strong to justify the use of $\delta^{18}O$ pattern matching across the entire period. We re-examined the tie points for intervals corresponding to correlation minima (e.g., 1979, 1963, 1962, 1943, 1942, 1924, 1921, 1903, 1904, and 1891). Adjusting tie-point depths within plausible bounds did not improve agreement during these intervals. These results indicate that the reduced correlation is mainly due to inherent differences between the model and ice-core records, rather than to systematic age-scale misalignment. The correlation varies over time and generally increases toward the present, implying improved model performance in recent decades. In particular, the correlation tends to deteriorate before 1940, coinciding with a marked increase in the ensemble spread of surface pressure in the 20CRv2 reanalysis (Compo et al., 2011), an indicator of reanalysis uncertainty (Fig. 3b). Thus, the lower correlation in earlier periods likely reflects the reduced quality of the reanalysis data at that time and may also reflect diffusion-induced smoothing in the ice core.

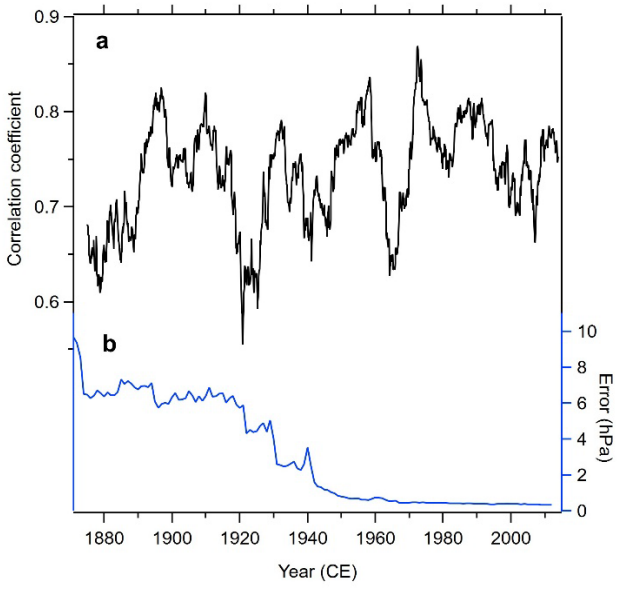

Figure 3. Model-data correlation and reanalysis uncertainty. (a) Running correlation coefficients between monthly $\delta^{18}O$ values of the SE2 ice core and isotope-enabled climate model simulations, using a 97-month window. (b) The ensemble spread of surface pressure from the 20CRv2 reanalysis averaged over the region 60–80°N, 90°W–0°, was used as a proxy for reconstruction uncertainty.

https://doi.org/10.5194/egusphere-2026-3602
Preprint. Discussion started: 9 July 2026

Melt layers and nuclear test markers support the accuracy of the SE2025iso age scale at seasonal to annual timescales. The 2012 and 1889 surface melt events (Nghiem et al., 2012; Keegan et al., 2014) correspond to melt layers at 15.42–16.09 m and 165.75–165.78 m (Kawakami et al., 2023), respectively, corresponding to February to July 2012 and August 1889 on the SE2025iso age scale. A tritium peak from the 1961–1962 H-bomb tests, typically appearing in 1963 ice cores (Clausen and Hammer, 1988), was found at 83.66–84.20 m in SE2 (Kawakami et al., 2023), corresponding to February to July 1963 on the SE2025iso age scale. These markers support the accuracy of the SE2025iso age scale.

Although an uncertainty estimation is difficult for the entire record, we performed an error evaluation under the following assumptions: (1) uncertainty associated with peak identification of the tie points was set to ±1 month, except for several ambiguous tie points where ±2 months was assigned; and (2) interpolation errors (95%-confidence limits) were estimated using a Monte Carlo simulation based on fitting ensembles of straight lines to subsets of the age data (Scholz and Hoffmann, 2011). Thus, the estimated uncertainty mainly reflects tie-point identification and interpolation uncertainty. The results indicate that the uncertainty ranges from 0.1 to 5.6 months (2.0 on average) (Fig. 4). For example, the interval from 1900 to 1910 CE exhibits the largest uncertainties—reaching 5 months—because of a limited number of tie points and rapid changes in the depth–age relationship in this part of the core. In contrast, periods with sufficient tie points show uncertainties of 1.4–2.7 months, indicating that the depth–age relationship is well constrained in most intervals.

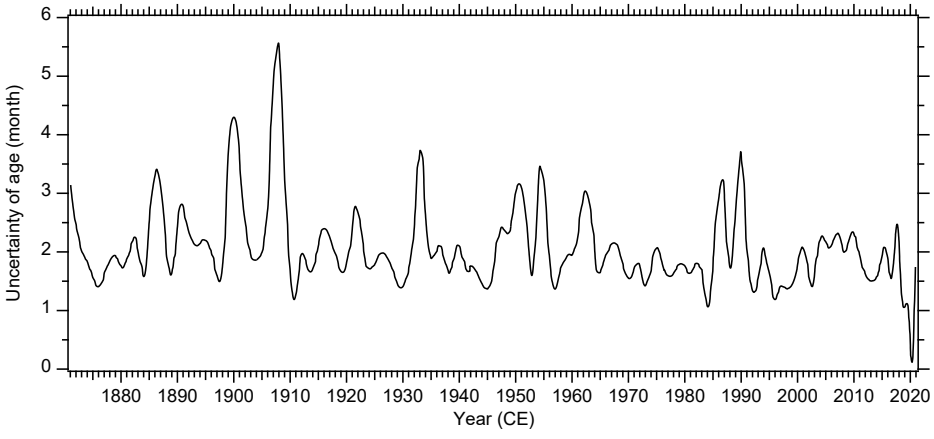

Figure 4. Age uncertainty of the SE2025iso age scale. The horizontal axis represents year (CE), and the vertical axis shows the age uncertainty (95% confidence limits) in months.

3.1.3 Post-Depositional Effects

An assessment of post-depositional effects on $\delta^{18}O$ signals at the SE-Dome site shows a negligible peak shift after snow deposition (Fig. 5). The simulation shows an average post-depositional impact on $\delta^{18}O$ due to vapor exchange of +1.7‰. The

https://doi.org/10.5194/egusphere-2026-3602
Preprint. Discussion started: 9 July 2026

interannual variability of $\delta^{18}O$ decreases slightly (a 23.5% decrease in annual variance). We also extracted all maxima and minima that could be identified in both the firn core simulation with and without post-depositional fractionation during vapor exchange. The results show that $\delta^{18}O$ peak shifts are -7.1 days and -4.9 days for summer and winter, respectively. Following recent recommendations (Ollivier et al., 2025a), we tested the sensitivity of the simulated post-depositional impact to the vertical grid resolution and found the results were robust. Finally, we also note that the model produces excessive smoothing at the SE site. As a result, the 1–3-month variability visible in the ice-core record is reduced (Fig. 5). This mismatch likely reflects limitations in the current post-depositional model for white-noise–related processes. In summary, post-depositional processes increase the $\delta^{18}O$ values of snow but do not substantially shift seasonal maxima and minima, supporting age determination by pattern matching between ice-core and model $\delta^{18}O$ records.

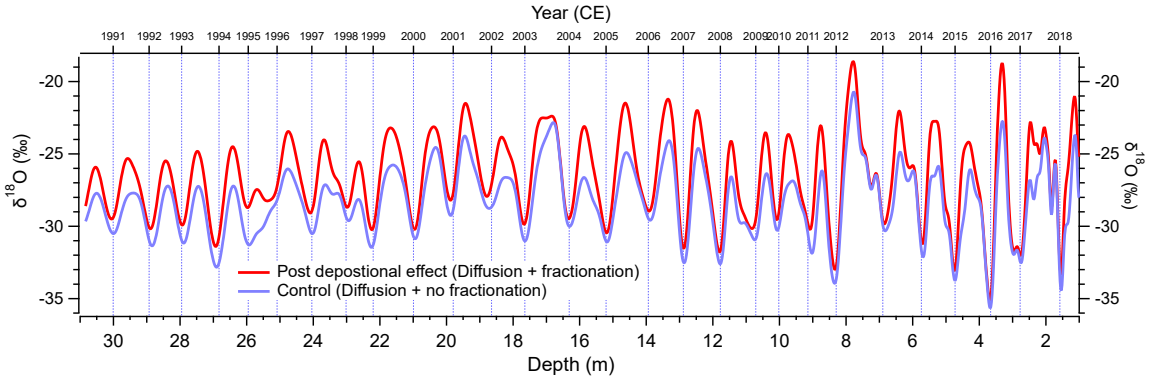

Figure 5. Modelled post-depositional effects on the SE-Dome ice-core $\delta^{18}O$ record. The blue line shows the result of the control experiment, including post-depositional diffusion but excluding isotope exchange between vapor and snow. The red line shows the experiment including both post-depositional diffusion and vapor–snow isotope exchange.

3.2 Multi-Month Variability of $\delta^{18}O$ in the SE2 Ice Core

3.2.1 Reproducibility of the SE-Dome $\delta^{18}O$ Records and Comparison with Other Greenland Cores

To evaluate the reproducibility of $\delta^{18}O$ records at SE-Dome, we first compared the $\delta^{18}O$ records of the SE1 and SE2 ice cores (Fig. 6). The correlation between SE1 and SE2 is exceptionally high (r = 0.90), indicating that fine-scale intra-annual signals are well preserved in both cores. In general, chemical proxies that reflect various aerosols exhibit spatial variability in ice cores. For example, a study of the NEEM ice core found that at least five ice cores were required to capture 70% of interannual atmospheric variability due to lower correlations among multiple ice cores from the same site (e.g., r = 0.7 for NH_4^+, r = 0.6 for NO_3^-, and r = 0.3 for Ca^{2+}, Na^+, and H_2O_2) (Gfeller et al., 2014). In contrast to these aerosol proxies, recent work has suggested that the $\delta^{18}O$ of snow is influenced by the $\delta^{18}O$ of atmospheric vapor through post-depositional snow–

https://doi.org/10.5194/egusphere-2026-3602
Preprint. Discussion started: 9 July 2026

vapor exchange (Dietrich et al., 2023). Because the vapor $\delta^{18}O$ is expected to be more spatially homogeneous than snow $\delta^{18}O$, such exchange may increase the representativeness of $\delta^{18}O$ signals in ice cores. The high reproducibility of $\delta^{18}O$ between SE1 and SE2 is consistent with this interpretation and suggests that $\delta^{18}O$ variability at SE-Dome is less affected by local noise.

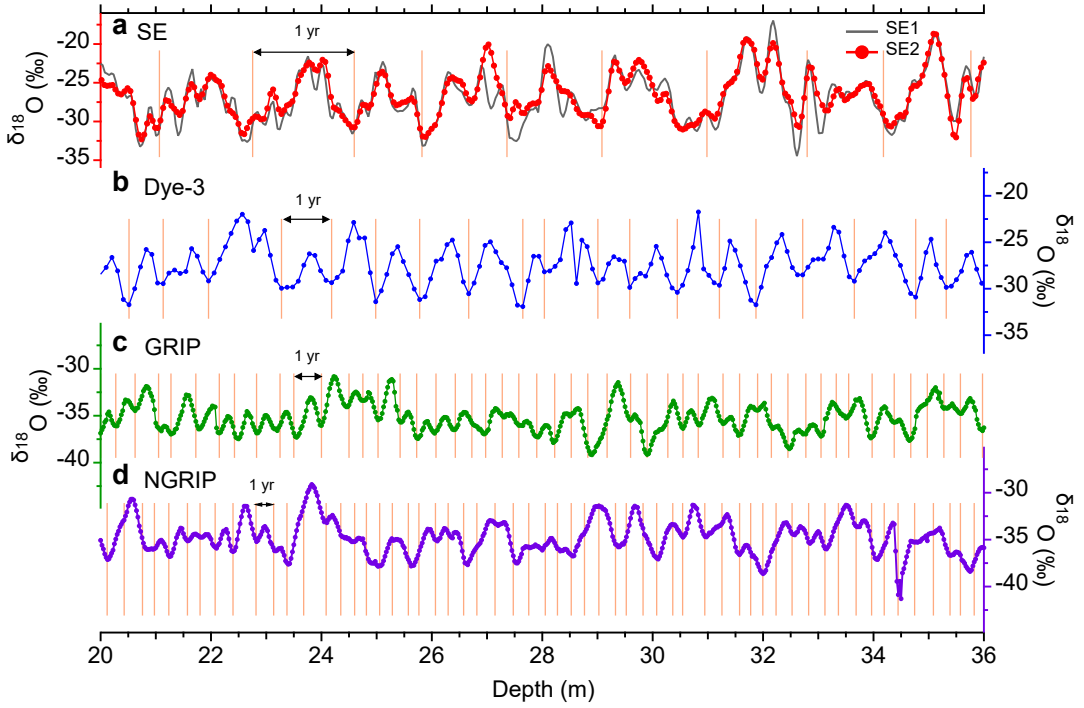

Figure 6. Differences in $\delta^{18}O$ signal smoothing across Greenland ice cores. (a) $\delta^{18}O$ records of SE1 (black) and SE2 (red) ice cores, with SE1 depth adjusted to match SE2. In this figure, the SE2 depth is shown relative to the top of the ice core, which is 1.27 m below the snow surface. (b–d) $\delta^{18}O$ profiles of Dye-3 (blue), GRIP (green), and NGRIP (purple). Dots show sampling resolutions for each core. Vertical orange bars mark annual layer boundaries. SE2 data follow the SE2025iso age scale, while Dye-3, GRIP, and NGRIP use the GICC21 chronology (Sinnl et al., 2022).

To examine how accumulation rate influences multi-month signal preservation, we compared $\delta^{18}O$ profiles of several Greenland ice cores at similar depths of 20–36 m (Fig. 6). Because the cores were drilled in different years, layers representing the same calendar year occur at different depths and experience different degrees of post-depositional vapor exchange and diffusion; therefore, we performed a depth-based comparison. The comparison shows that the SE2 core exhibits larger amplitude and more pronounced multi-month $\delta^{18}O$ variability relative to other Greenland ice cores (Fig. 6). The smooth continuity between adjacent measurements suggests that short-period variability has been attenuated and is not limited by sampling resolution. First, the SE2 core shows the largest $\delta^{18}O$ variability (2σ) of ±6.9‰ among these cores, compared to ±4.3‰, ±3.7‰, and ±3.4‰ for Dye-3, GRIP, and NGRIP, respectively. Assuming that the seasonal $\delta^{18}O$

https://doi.org/10.5194/egusphere-2026-3602
Preprint. Discussion started: 9 July 2026

amplitude of precipitation is of similar magnitude among the Greenland sites (e.g., −45‰ to −30‰ at NGRIP; Bory et al. 2002), the larger variability preserved in the SE2 core indicates weaker attenuation relative to the lower-accumulation sites. This result is consistent with the expectation that high-accumulation sites experience weaker diffusive smoothing (e.g., Cuffey and Steig, 1998). Second, SE2 displays more frequent multi-month $\delta^{18}O$ variability. In NGRIP and GRIP, $\delta^{18}O$ follows a simple seasonal pattern with a single peak per year, showing summer maxima and winter minima. Dye-3 occasionally displays two peaks per year. In contrast, SE2 frequently exhibits multiple peaks within a single year. The accumulation rates of SE2 (Iizuka et al., 2021), Dye-3 (Herron et al., 1981), GRIP (Johnsen et al., 1992), and NGRIP (NGRIP members, 2004) are 1.02, 0.55, 0.23, and 0.19 m yr^{-1}, respectively, indicating that higher accumulation rates enhance the preservation of intra-annual variations in SE2.

3.2.2 Intra-Annual $\delta^{18}O$ Structure and Implications for Dating

To evaluate the applicability of automated annual layer counting methods (Winstrup et al., 2012) to the SE2 $\delta^{18}O$ record, we conducted principal component analysis (PCA) on data from 1975 to 2005 CE (Fig. 7). Note that the PCA is applied to the $\delta^{18}O$ record on the SE2025iso age scale, and the PCA is not used to construct the age model for the SE2 core. PC1 explains 57.9% of the variance and captures the primary seasonal cycle, peaking in July in agreement with summer temperature maxima. However, PC1 alone does not resolve the detailed intra-annual structure required for dating with multi-month precision. PC3 (7.8%) and PC4 (4.4%) display multiple peaks and troughs with distinct phase relationships across the year. These components are consistently observed and exhibit reproducible phase structures across years. Their reproduction in $\delta^{18}O$ model outputs indicates that the multi-month-scale variations likely reflect atmospheric processes rather than random noise. Preliminary analysis of IsoGSM shows that some events appear to be linked to synoptic-scale low-pressure systems over the ocean south of Greenland, but others are not, implying multiple controlling factors behind the multi-month-scale variations. Although a detailed investigation of the mechanism of this phenomenon is beyond the scope of this study, these results indicate that this intra-annual structure can be used for fine-scale age development. When we applied the automatic counting method (Winstrup et al., 2012) to the SE2 $\delta^{18}O$ record, the resulting annual layer counts showed cumulative age errors of up to ±3 years below 150 m depth. This error represents the statistical uncertainty estimated by the counting algorithm, not a comparison with independent age markers. A comparable PCA analysis performed for Dye-3, GRIP, and NGRIP over near-surface ca. 30-year intervals shows that the PC3 and PC4 components are weaker in those cores (Fig. A1), suggesting that SE2 exhibits a more pronounced multi-month structure than the other cores examined here.

https://doi.org/10.5194/egusphere-2026-3602
Preprint. Discussion started: 9 July 2026

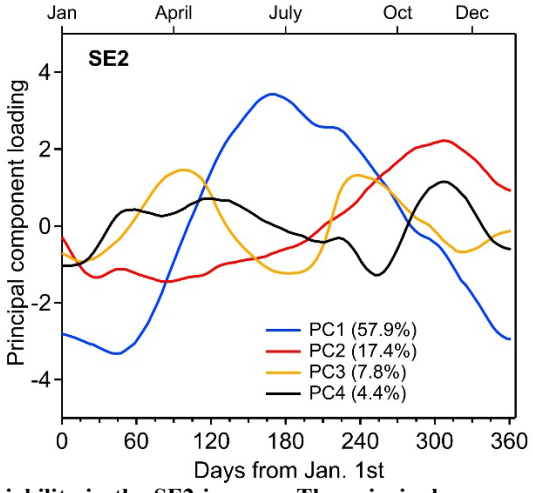

Figure 7. Intra-annual pattern of $\delta^{18}O$ variability in the SE2 ice core. The principal component scores of PC1 (blue), PC2 (red), PC3 (yellow), and PC4 (black) for $\delta^{18}O$ variations are shown.

3.3 Snow Accumulation at the SE-Dome Site

3.3.1 Reconstructed Accumulation Rates

The SE2025iso age scale enables the reconstruction of long-term snow accumulation rates at the SE-Dome site. Fig. 8 presents the annual and seasonal accumulation rates from 1872 to 2019 CE. The mean yearly accumulation rate over this period is 1.08 m w.e. yr^{-1}, with interannual variability ranging from 0.58 to 1.60 m w.e. yr^{-1}. The mean accumulation rates of SE1 and SE2 are correlated (r = 0.67), indicating general consistency between the two cores for annual-average data. Seasonal accumulation rates are 0.27, 0.26, 0.26, and 0.29 m w.e. yr^{-1} in spring (MAM), summer (JJA), autumn (SON), and winter (DJF), respectively, indicating that snowfall is relatively evenly distributed throughout the year. This balanced accumulation likely reduces seasonal bias in proxies deposited mainly through wet deposition. No significant long-term trend over the entire record is detected in annual accumulation rates, suggesting that mean snowfall levels have remained stable. However, slight trends may arise depending on the assumed ice-sheet thickness used for thinning correction (see Sect. 2.5), requiring caution when interpreting long-term accumulation trends.

https://doi.org/10.5194/egusphere-2026-3602
Preprint. Discussion started: 9 July 2026

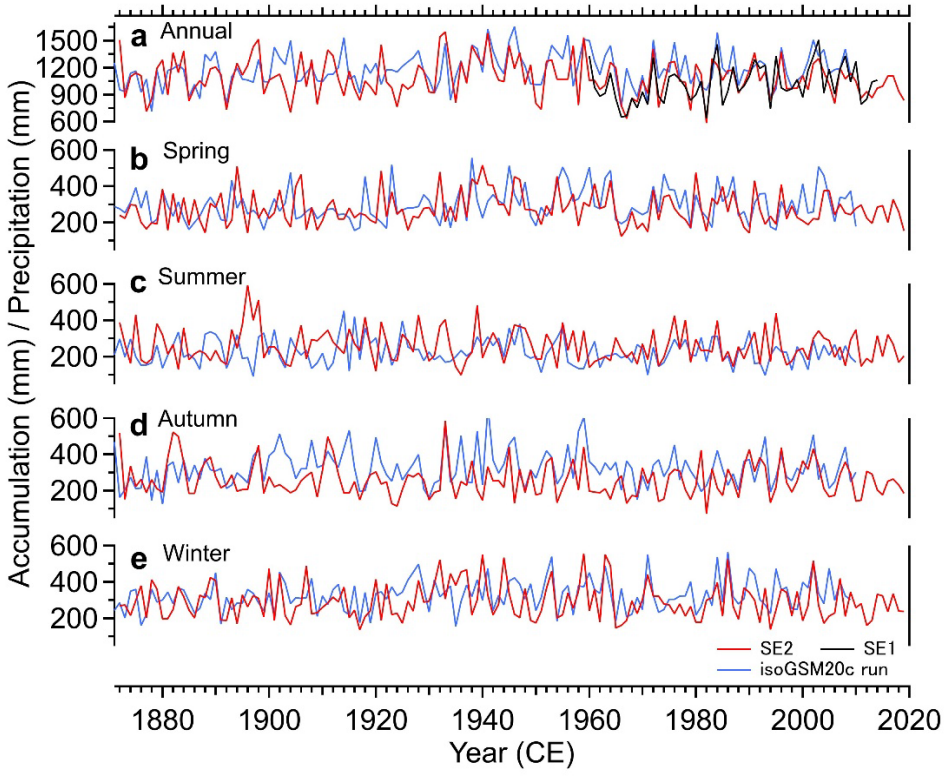

Figure 8. Accumulation rates reconstructed from SE2 ice core (red) and precipitation data of IsoGSM20c run (blue). Panel (a) shows annual accumulation, and panels (b), (c), (d), and (e) show seasonal accumulation for spring, summer, autumn, and winter, respectively. Accumulation rate from SE1 ice core (Furukawa et al., 2017) is also shown in (a) (black).

https://doi.org/10.5194/egusphere-2026-3602
Preprint. Discussion started: 9 July 2026

3.3.2 Seasonal Accumulation Regime

The ice-core-derived accumulation rates are compared with precipitation from reanalysis datasets (Table 1). Because accumulation rates are calculated from layer thicknesses based on the SE2 chronology, this comparison can be used both to assess the chronology and to characterize the accumulation regime at SE-Dome. The SE2 accumulation rates show statistically significant correlations with ERA5 precipitation at the annual scale and in all seasons, although the summer correlation is weak ($r = 0.21$, $p < 0.05$; Table 1). For the extended period covered by the IsoGSM20c run (1871–2010 CE), significant correlations are obtained at the annual scale and in all seasons except summer. Note that the IsoGSM20c precipitation is similar to the 20CRv2 dataset because the IsoGSM20c run uses the incremental correction method (Yoshimura and Kanamitsu, 2013).

Table 1. Correlation coefficients and mean accumulation rates. Top section: Correlation coefficients (r) between accumulation rates from SE2 ice core and precipitation data. Bottom section: Mean accumulation rates (m yr^{-1}) from ice cores and mean precipitation values (m yr^{-1}) from the reanalysis datasets.

	Annual	Spring	Summer	Autumn	Winter
Correlation coefficient (r) between SE2 accumulation rate vs. precipitation amount					
SE2-core vs ERA5 (1940-2020 CE)	0.68**	0.32**	0.21*	0.44**	0.54**
SE2-core vs IsoGSM20c run (1871-2010 CE)	0.38**	0.25**	0.09	0.29**	0.38**
Accumulation rate (m yr^{-1}) and precipitation (m yr^{-1})					
SE2 core (1940-2020 CE)	1.07	0.28	0.25	0.25	0.29
SE2 core (1871-2020 CE)	1.08	0.27	0.26	0.26	0.29
ERA5 (1940-2020 CE)	0.86	0.20	0.13	0.24	0.29
IsoGSM20c run (1871-2010 CE)	1.17	0.30	0.23	0.32	0.33

(p<0.01, *p<0.05)**

Seasonal mean accumulation rates also indicate model and reanalysis biases. Both ERA5 and IsoGSM20c run datasets show relatively low summer precipitation compared to other seasons (the bottom section of Table 1), suggesting that these datasets may underestimate summer accumulation at this site. This summer underestimation is consistent with previous findings from

https://doi.org/10.5194/egusphere-2026-3602
Preprint. Discussion started: 9 July 2026

the SE1 core (Furukawa et al., 2017), and the SE2 record extends this evidence back to 1871 CE. Reproducing seasonal accumulation at the SE-Dome site remains challenging for climate models due to steep spatial gradients in coastal precipitation (Fig. 1). Seasonal differences in precipitation across the Greenland Ice Sheet are characterized by distinct patterns: summer-dominated accumulation in the northwest, weak seasonal accumulation in the central region, and winter-dominated accumulation in the southeast (Fig. 9). Although ERA5 has been shown to reproduce the large-scale spatial distribution of decadal-mean accumulation across Greenland (Schneider et al., 2023), our analysis focuses on seasonal variability. In the ERA5 data, SE-Dome is located within the winter-dominated accumulation region of southeastern Greenland, resulting in relatively low summer precipitation at the site (Fig. 9). In contrast, the SE2 core data indicate nearly uniform accumulation throughout the year, suggesting that SE-Dome is better characterized as a transition site between summer- and winter-dominated accumulation regimes. The SE2 record therefore provides an important benchmark for evaluating model performance in regions with strong spatial gradients in seasonal precipitation.

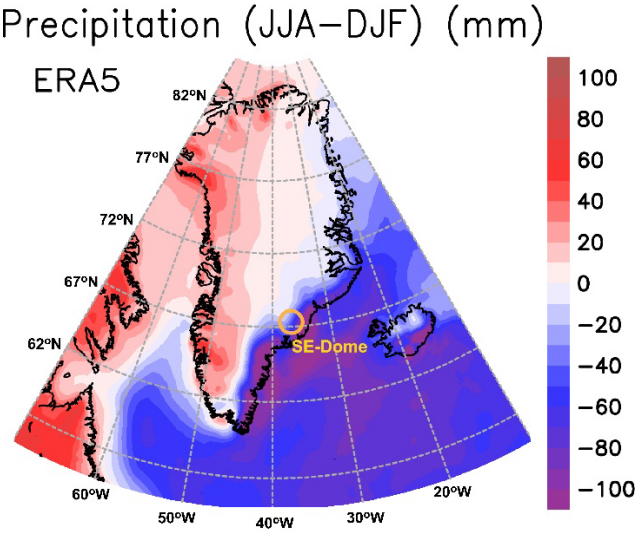

Figure 9. Spatial distribution of seasonal precipitation differences over Greenland. The color scale shows the difference in precipitation between summer (JJA) and winter (DJF) based on ERA5 over 1979-2014 CE. Positive values indicate a higher accumulation rate in summer than in winter. The circle symbol indicates the SE-Dome site.

Seasonal contrasts in snow accumulation across the Greenland Ice Sheet result from regional differences in atmospheric circulation and moisture transport pathways (Fig. 10). During summer, the western side of Greenland is characterized by prevailing southerly winds from the ocean in the lower atmosphere (Schuenemann et al., 2009; Mattingly et al., 2020), which favor orographic precipitation. In contrast, the eastern side is characterized by either prevailing winds from the interior or weak background flow under the influence of an orographically induced anticyclone. During winter, cold winds from the interior prevail over the western side, resulting in conditions unfavorable for precipitation. Meanwhile, the southeastern side lies north of the storm track of extratropical cyclones, where easterly winds prevail (Schuenemann et al., 2009) and provide

https://doi.org/10.5194/egusphere-2026-3602
Preprint. Discussion started: 9 July 2026

favorable conditions for orographic precipitation. These contrasting seasonal circulation regimes create spatial gradients in accumulation seasonality and establish a transition zone across the ice sheet. SE-Dome appears to lie near the transition between them.

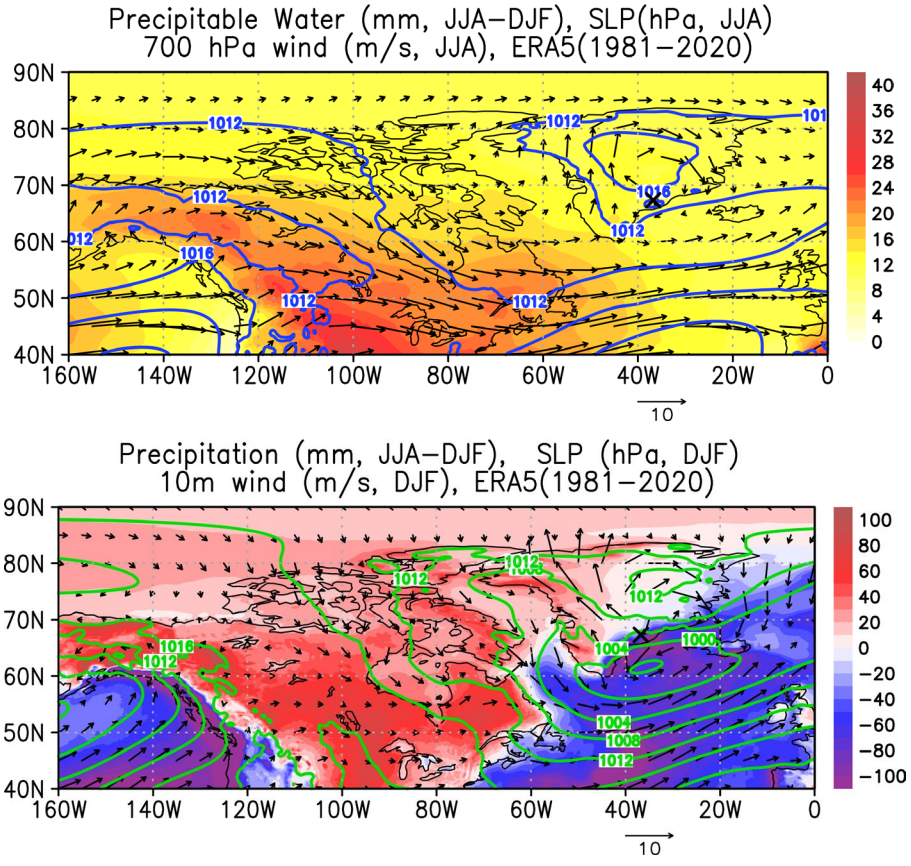

Figure 10. Atmospheric circulation and moisture transport over Greenland and the surrounding region. Upper panel: Seasonal difference in precipitable water (JJA−DJF; color), mean sea level pressure in summer (JJA; contours), and 700 hPa wind vectors in summer (JJA; arrows). Lower panel: Seasonal difference in precipitation (JJA−DJF; color), mean sea level pressure in winter (DJF; contours), and 10 m wind vectors in winter (DJF; arrows).

Interpretation of such seasonal accumulation patterns is often limited by temporal resolution and chronological uncertainty. A recent synthesis showed that about 80% of accumulation records represent annual or multi-annual averages, whereas sub-annual constraints remain scarce and often rely on simplified seasonal-layer identification (Lindsey-Clark et al., 2026). In the SE2 record, no multi-decadal interval exhibits persistently greater accumulation in either summer or winter. This result indicates that the balanced seasonal accumulation regime at SE-Dome, a site near the transition between contrasting accumulation regimes across Greenland, has been maintained throughout the past 150 years. This persistence also suggests

https://doi.org/10.5194/egusphere-2026-3602
Preprint. Discussion started: 9 July 2026

that the atmospheric circulation and moisture transport balance responsible for the weak seasonality at this site did not change substantially over this interval, despite recent Arctic warming.

3.4 Consistency Checks and Applications of the SE2025iso Age Scale

3.4.1 Seasonal Pattern of H_2O_2 Concentrations

As an example of applying the SE2025iso age scale to a chemical proxy, we analyzed previously published H_2O_2 data from the SE2 core (Kawakami et al., 2023). In constructing the SE2025iso age scale, H_2O_2 seasonality was used only as a secondary constraint for limited sections, and H_2O_2 peaks were not forced to align with the summer solstice or any prescribed date. We therefore use SE2025iso to evaluate the mean seasonal pattern of H_2O_2 concentrations obtained by compositing the H_2O_2 records. On the SE2025iso age scale, mean H_2O_2 concentrations reach their maximum and minimum on 12 July and 4 January, respectively, with standard deviations of 29 and 28 days (Fig. 11). Generally, H_2O_2 is primarily formed by photochemical reactions (Frey et al., 2005; Sakugawa et al., 2002), and its maxima and minima are thought to correspond approximately to the summer and winter, respectively (Mosley-Thompson et al., 2001). Our results are consistent with previous studies reporting that the maxima and minima of H_2O_2 concentrations in Greenland ice cores occur in July and January, respectively (Steen-Larsen et al., 2011; Gfeller et al., 2014). However, our previous age scale, SE2time2023, was constructed assuming that the H_2O_2 maxima and minima correspond to the summer and winter solstices, respectively (Kawakami et al., 2023). Therefore, the dating of H_2O_2 maxima and minima on the SE2025iso age scale is delayed by ca. 2-3 weeks compared to the previous H_2O_2-based age scale, SE2time2023 (Kawakami et al., 2023).

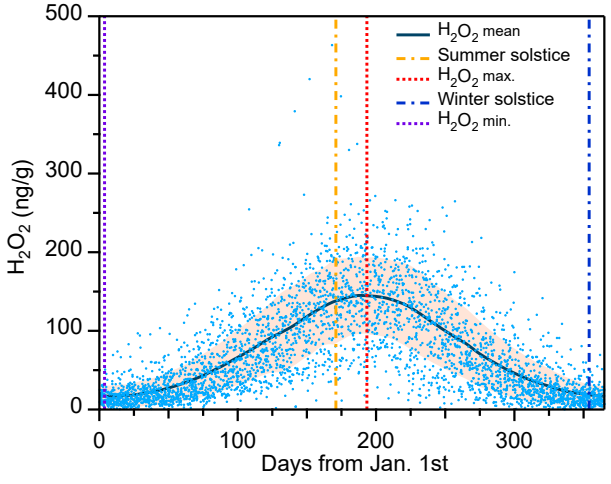

Figure 11. Climatological seasonal pattern of H_2O_2 with SE2025iso. A composite of SE2 core H_2O_2 concentrations over the past 150 years, plotted against months. Blue dots indicate individual H_2O_2 concentration values. The blue line and the orange shading represent the mean seasonal trend and its interannual variability (±1σ), respectively. Yellow and blue dashed-dotted lines show the summer and winter solstices, respectively. Orange and purple dashed lines indicate the maxima and minima of H_2O_2 concentrations, respectively.

https://doi.org/10.5194/egusphere-2026-3602
Preprint. Discussion started: 9 July 2026

3.4.2 Multi-Month Features of Volcanic Sulfate Deposition

To evaluate the consistency of SE2025iso with existing Greenland ice core chronologies, we compared the SE2025iso timescale with the NEEM-S1 timescale (Sigl et al., 2013; Sigl et al., 2015) using volcanic reference layers. Ten volcanic eruptions were identified in the NEEM-S1 ice core after 1871 CE (Sigl et al., 2013). We detected eight nss-SO_4^{2-} peaks from significant eruptions, confirming the annual consistency between SE2025iso and NEEM-S1. These eruptions and their corresponding years are as follows: Pinatubo (1992 CE, Indonesia), Agung (1964 CE, Indonesia), Bezymianny (1957 CE in Kamchatka), Hekla (1947 CE, Iceland), Katla (1918 CE, Iceland), Katmai (1912 CE, Alaska), Ksudach (1908 CE, Kamchatka), and Krakatoa (1883 CE, Indonesia). For Bezymianny (1957 CE), no peak was detected in the annual mean nss-SO_4^{2-} data, but a significant short-lived peak was observed in the raw and monthly-averaged data. Sulfate peaks associated with Raikoke (1924–1927 CE, Kuril Islands) and Grimsvøtn (1872 CE, Iceland) were not detected in the SE2 core. These two eruptions were relatively high-latitude and moderate in magnitude, which may have resulted in site-specific differences in sulfate deposition due to variations in atmospheric transport pathways. Note that the NEEM-S1 timescale (Sigl et al., 2013; Sigl et al., 2015) is linked to the NGRIP chronology (Vinther et al., 2006) through volcanic reference horizons, which are observed in NGRIP sulfate records (Plummer et al., 2012). Thus, the agreement of volcanic horizons indicates that the SE2025iso age scale is consistent with the Greenland ice-core chronology framework for major volcanic events. Having established this annual-scale consistency, we then used the multi-month resolution of SE2025iso to examine the detailed structure of volcanic sulfate deposition.

High-resolution sulfate records from the SE2 ice core reveal distinct deposition patterns. Among the volcanic signals, five eruptions from remote regions—Pinatubo, Agung, Krakatoa, Bezymianny, and Ksudach—exhibit similar features in the SE2 core. Comparisons of these five volcanic signals in NEEM-2011-S1 (nss-Sulfur), NGRIP (Sulfur), and SE2 cores (nss-SO_4^{2-}) are shown in Fig. 12. The eruption dates shown in Fig. 12 were based on the Smithsonian Institution's Global Volcanism Program database (Global Volcanism Program, 2024). In the SE2 nss-SO_4^{2-} record, these eruptions are characterized by a narrow sulfate peak lasting approximately 2 months and delayed by ca. 1.5 years after the eruption. This structure is reproducible across these five events in SE2, whereas similar features are not apparent in the NEEM or NGRIP records, likely due to their lower temporal resolution.

https://doi.org/10.5194/egusphere-2026-3602
Preprint. Discussion started: 9 July 2026

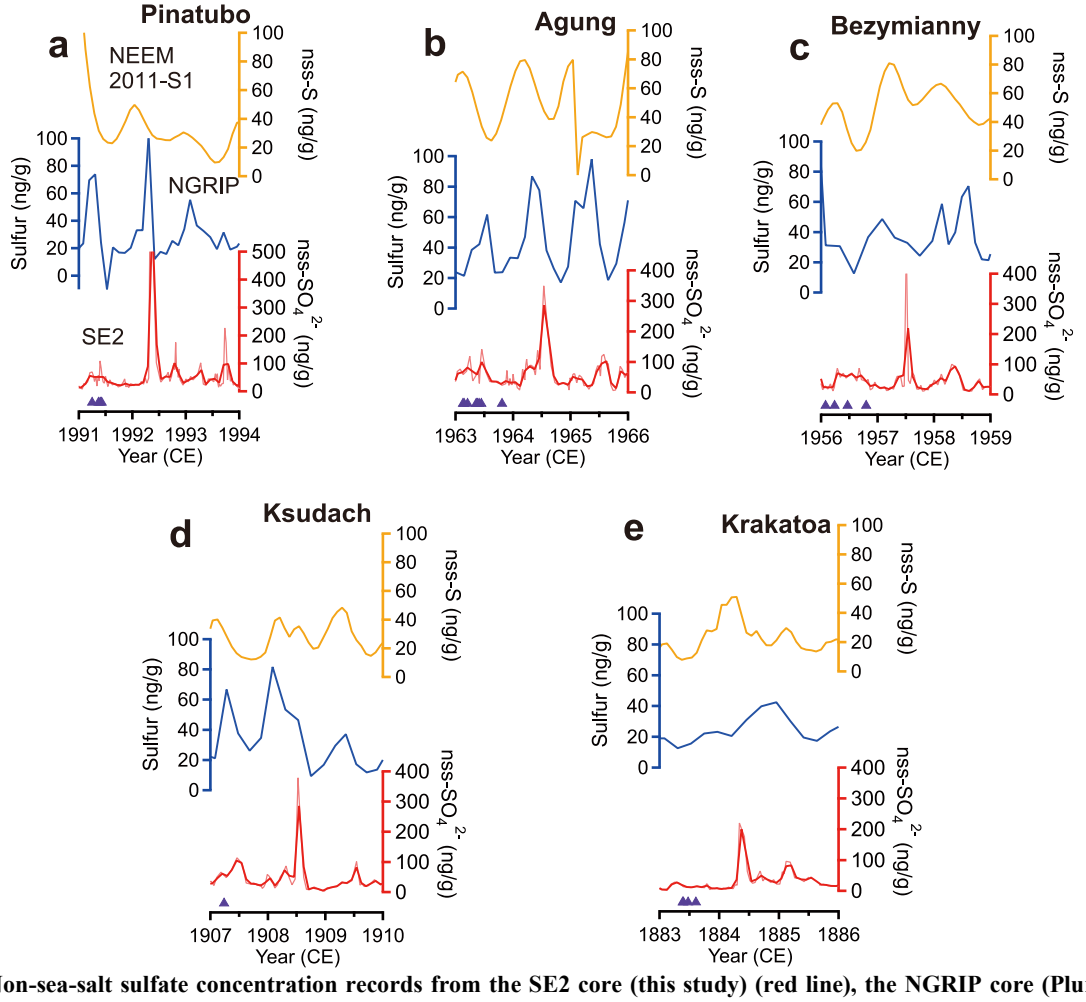

Figure 12. Non-sea-salt sulfate concentration records from the SE2 core (this study) (red line), the NGRIP core (Plummer et al., 2012; Sigl et al., 2015) (blue line), and the NEEM-2011-S1 core (Sigl et al., 2015) (yellow line). Panels (a), (b), (c), (d), and (e) show each volcanic eruption event for Pinatubo, Agung, Bezymianny, Ksudach, and Krakatoa. The NGRIP and NEEM-2011-S1 data were plotted on the NS1-2011 time scale (Sigl et al., 2015). Thick lines are monthly data. The purple triangle at the bottom shows the dates of volcanic eruptions.

To investigate the timing of sulfate deposition with multi-month resolution, we conducted two analyses using the SE2025iso age scale (Fig. 13). The first approach aligned the nss-SO_4^{2-} records from each eruption by setting the major eruption date as day zero. Although explosive eruptions involve multiple events, we assigned the first significant eruption as the start date: June for Pinatubo, March for Agung, March for Bezymianny, March for Ksudach, and May for Krakatoa. The results showed substantial variability in the timing of sulfate peaks (Fig. 13a). Notably, Agung is delayed relative to Krakatoa despite their similar latitudes. These results indicate that the transport and deposition time to SE-Dome differs among eruptions. In the second approach, we plotted the data relative to January of the eruption year. For example, for the June 1991 Pinatubo eruption, the monthly records were plotted relative to January 1991 (Fig. 13b). This method aligns the

https://doi.org/10.5194/egusphere-2026-3602
Preprint. Discussion started: 9 July 2026

horizontal axis by month, allowing direct comparison of seasonal patterns. Because sulfate aerosols also include biogenic sources and tend to peak in summer, this analysis helps distinguish background seasonality from eruption-related signals. Sulfate peaks associated with major eruptions consistently appeared from April to July of the following year (Fig. 13b). To clarify this seasonal pattern, we constructed a composite profile based on the calendar-aligned data (Fig. A2). The composite shows a background seasonal cycle and a sharp nss-SO_4^{2-} peak in the summer following each eruption. The repeated occurrence of sulfate peaks following major eruptions indicates that the SE2 record preserves a reproducible seasonal structure in post-eruption sulfate deposition. The present data do not distinguish among stratospheric transport, stratosphere–troposphere exchange, and oxidation, but they provide a high-resolution target for evaluating these processes in aerosol-transport models.

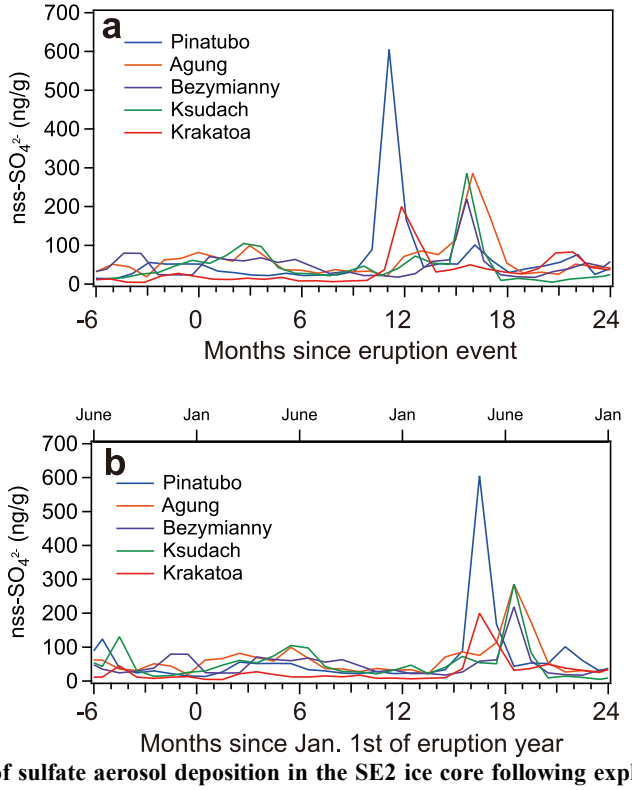

Figure 13. Monthly-resolution timing of sulfate aerosol deposition in the SE2 ice core following explosive eruptions. (a) The time series is aligned to the eruption date for each event. (b) The time series is aligned to January of the eruption year, enabling a comparison of seasonal deposition timing across events.

4 Conclusions

This study presented a new $\delta^{18}O$ record from the SE2 ice core and developed its age scale (SE2025iso) for 1871–2020 CE with multi-month precision by synchronizing isotope records between the SE2 ice core and climate models. The SE2 core

https://doi.org/10.5194/egusphere-2026-3602
Preprint. Discussion started: 9 July 2026

preserves clear intra-annual signals formed by large-scale atmospheric circulation, enabling the development of this high-resolution age scale beyond seasonal extremes. Because there are no absolute monthly markers, strict tests of monthly absolute accuracy are not possible. However, we evaluated the chronology by comparing ice-core-derived snow accumulation with model/reanalysis precipitation at the seasonal scale and volcanic timings with established Greenland ice-core chronologies at the annual scale. The reconstructed accumulation rates correlate well with model precipitation data, except in summer, and their seasonal means indicate that reanalysis data underestimate summer precipitation at SE-Dome. The weak seasonality in accumulation at SE-Dome persisted throughout the past 150 years, implying that the atmospheric circulation and moisture-transport balance near the boundary between summer- and winter-dominated accumulation regimes across Greenland remained broadly stable despite recent Arctic warming. Applying SE2025iso to H_2O_2 data identified seasonal maxima and minima on 12 July and 4 January, respectively, suggesting a temporal lag in the deposition of photochemically reactive species. Finally, the SE2 core record exhibits distinct multi-month features in volcanic sulfate deposition, suggesting complexity in the transport and deposition of volcanic sulfate. These findings demonstrate that high-accumulation Greenland ice cores can preserve reproducible multi-month isotope variability and that SE2025iso provides a chronological framework for investigating sub-annual proxy variability and deposition processes in southeast Greenland.

Data availability

The SE2 $\delta^{18}O$ data and the SE2025iso age-scale dataset, including the tie points used for age-scale construction, are available from the Hokkaido University Collection of Scholarly and Academic Papers at https://doi.org/10.14943/2115.98166. The same dataset will also be archived in the NOAA/WDS Paleoclimatology database before final publication at https://www.ncei.noaa.gov/access/paleo-search/study/41203.

https://doi.org/10.5194/egusphere-2026-3602
Preprint. Discussion started: 9 July 2026

Appendix A

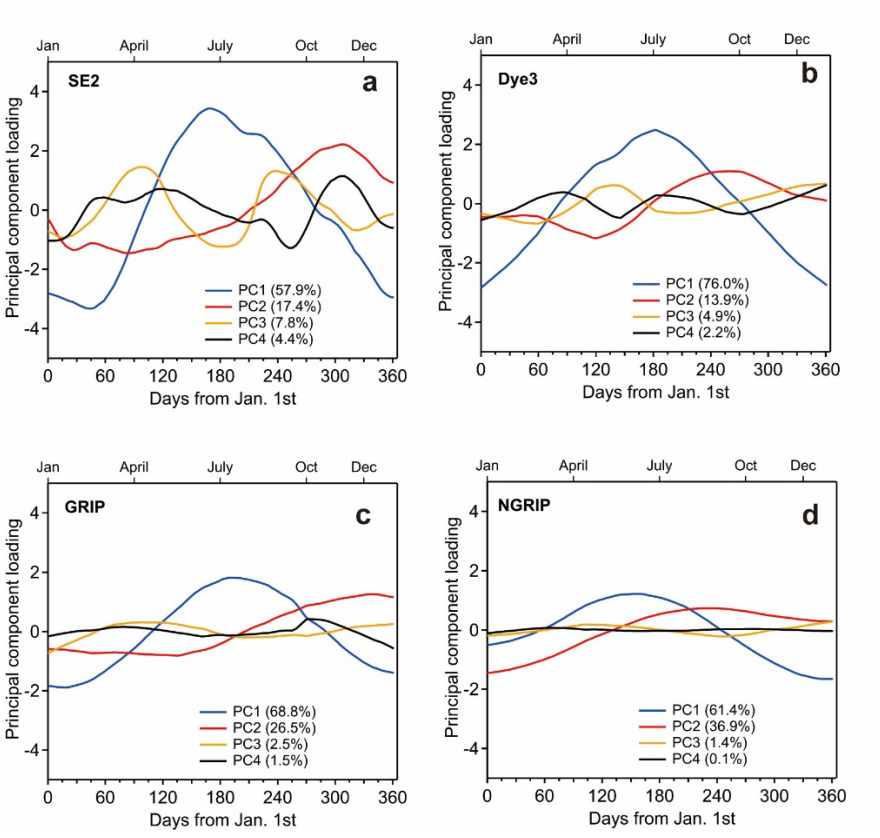

Figure A1. Principal component analysis (PCA) of seasonal $\delta^{18}O$ variability in four Greenland ice cores. Principal component loadings (PC1–PC4) are shown as a function of day of year. Panels (a), (b), (c), and (d) show the results for SE2, Dye3, GRIP, and NGRIP ice cores, respectively. Percent variance explained by each component is indicated in parentheses. To ensure comparable diffusion effects among sites, PCA was performed on near-surface intervals of approximately 30 years in length: 1975–2005 (SE2), 1982–1950 (Dye-3), 1980–1950 (GRIP), and 1973–1940 (NGRIP). PC3 and PC4 represent multi-month variability and account for a larger fraction of total variance in SE2 than in the other cores, consistent with enhanced preservation of sub-seasonal $\delta^{18}O$ variability at the high-accumulation SE2 site.

https://doi.org/10.5194/egusphere-2026-3602
Preprint. Discussion started: 9 July 2026

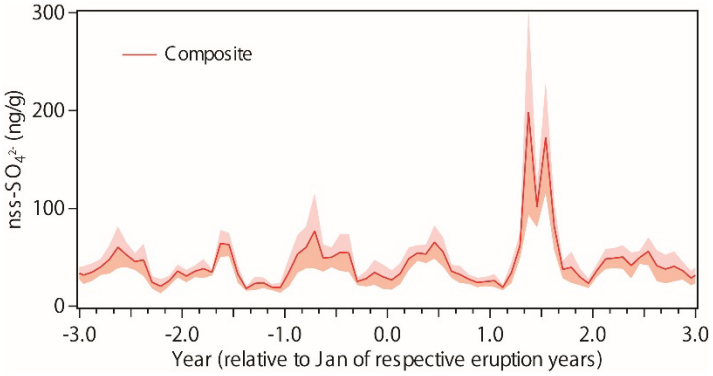

Figure A2. Composite of the aligned sulfate data shown in Fig. 13b.

Author contribution

R.U. planned and supervised this study. S.H. and R.U. contributed to the measurement of stable isotopes. H.B., K.Y., and A.O. provided isotope GCM datasets, and T.A. provided the accumulation data of reanalysis datasets. L.D. and H.C.S.-L. conducted post-depositional modelling analysis. S.H. and R.U. conducted the data analyses. S.H. and R.U. wrote the original draft. S.H., T.A., and R.U. prepared the figures. R.U. wrote the manuscript. Y.I., S.M., K.K., and M.M. contributed to SE2 core project administration. R.U. and Y.I. acquired the funding. All the authors provided comments on the manuscript.

Competing interests

The authors declare that they have no conflict of interest.

Acknowledgements

We sincerely thank the SE2 core project members, especially M. Sasage and T. Saito, for their efforts in sample preparation. We further acknowledge H. Uema, K. Osawa, and R. Hoshiya for their contributions to the isotope measurements. We thank R. Furukawa for his work on dating validation. We appreciate S. Ishino, A. Hori, K. Horiuchi, T. Aoki, M. Niwano, N. Esashi, K. Fujita, T. Nakatsuka, and O. Abe for their insightful discussions. Artificial intelligence support: ChatGPT was used to assist with English-language editing. The authors reviewed and approved all text.

https://doi.org/10.5194/egusphere-2026-3602
Preprint. Discussion started: 9 July 2026

Financial support

This study was supported by JSPS KAKENHI (23K18518 for RU, 18H05292 for YI, 23H00511 for YI), the Arctic Challenge for Sustainability II (ArCS II) project (Program Grant Number JPMXD1420318865), and Kurita Water and Environment Foundation (22D008 for RU).

References

Alley, R. B., Shuman, C. A., Meese, D. A., Gow, A. J., Taylor, K. C., Cuffey, K. M., Fitzpatrick, J. J., Grootes, P. M., Zielinski, G. A., Ram, M., Spinelli, G., and Elder, B.: Visual-stratigraphic dating of the GISP2 ice core: Basis, reproducibility, and application, Journal of Geophysical Research: Oceans, 102, 26367-26381, 10.1029/96jc03837, 1997.

Andersen, K. K., Svensson, A., Johnsen, S. J., Rasmussen, S. O., Bigler, M., Röthlisberger, R., Ruth, U., Siggaard-Andersen, M.-L., Peder Steffensen, J., and Dahl-Jensen, D.: The Greenland Ice Core Chronology 2005, 15–42ka. Part 1: constructing the time scale, Quaternary Sci Rev, 25, 3246-3257, 10.1016/j.quascirev.2006.08.002, 2006.

Bong, H., Cauquoin, A., Okazaki, A., Chang, E. C., Werner, M., Wei, Z., Yeo, N., and Yoshimura, K.: Process-Based Intercomparison of Water Isotope-Enabled Models and Reanalysis Nudging Effects, Journal of Geophysical Research: Atmospheres, 129, 10.1029/2023jd038719, 2024.

Bory, A. J. M., Biscaye, P. E., Svensson, A., and Grousset, F. E.: Seasonal variability in the origin of recent atmospheric mineral dust at NorthGRIP, Greenland, Earth Planet Sc Lett, 196, 123-134, 10.1016/s0012-821x(01)00609-4, 2002.

Cauquoin, A. and Werner, M.: High-Resolution Nudged Isotope Modeling With ECHAM6-Wiso: Impacts of Updated Model Physics and ERA5 Reanalysis Data, Journal of Advances in Modeling Earth Systems, 13, 10.1029/2021ms002532, 2021.

Clausen, H. B. and Hammer, C. U.: The Laki and Tambora Eruptions as Revealed in Greenland Ice Cores from 11 Locations, Annals of Glaciology, 10, 16-22, 10.3189/s0260305500004092, 1988.

Compo, G. P., Whitaker, J. S., Sardeshmukh, P. D., Matsui, N., Allan, R. J., Yin, X., Gleason, B. E., Vose, R. S., Rutledge, G., Bessemoulin, P., Brönnimann, S., Brunet, M., Crouthamel, R. I., Grant, A. N., Groisman, P. Y., Jones, P. D., Kruk, M. C., Kruger, A. C., Marshall, G. J., Maugeri, M., Mok, H. Y., Nordli, Ø., Ross, T. F., Trigo, R. M., Wang, X. L., Woodruff, S. D., and Worley, S. J.: The Twentieth Century Reanalysis Project, Quarterly Journal of the Royal Meteorological Society, 137, 1-28, 10.1002/qj.776, 2011.

Cuffey, K. M. and Steig, E. J.: Isotopic diffusion in polar firn: implications for interpretation of seasonal climate parameters in ice-core records, with emphasis on central Greenland, Journal of Glaciology, 44, 273-284, 10.3189/s0022143000002616, 1998.

Dietrich, L. J., Steen-Larsen, H. C., Wahl, S., Faber, A.-K., and Fettweis, X.: On the importance of the humidity flux for the surface mass balance in the accumulation zone of the Greenland Ice Sheet, The Cryosphere, 18, 289-305, 10.5194/tc-18-289-2024, 2024.

Dietrich, L. J., Steen-Larsen, H. C., Wahl, S., Jones, T. R., Town, M. S., and Werner, M.: Snow-Atmosphere Humidity Exchange at the Ice Sheet Surface Alters Annual Mean Climate Signals in Ice Core Records, Geophys Res Lett, 50, 10.1029/2023gl104249, 2023.

Frey, M. M., Stewart, R. W., McConnell, J. R., and Bales, R. C.: Atmospheric hydroperoxides in West Antarctica: Links to stratospheric ozone and atmospheric oxidation capacity, Journal of Geophysical Research: Atmospheres, 110, 10.1029/2005jd006110, 2005.

Furukawa, R., Uemura, R., Fujita, K., Sjolte, J., Yoshimura, K., Matoba, S., and Iizuka, Y.: Seasonal-Scale Dating of a Shallow Ice Core From Greenland Using Oxygen Isotope Matching Between Data and Simulation, Journal of Geophysical Research: Atmospheres, 122, 10.1002/2017jd026716, 2017.

Gfeller, G., Fischer, H., Bigler, M., Schüpbach, S., Leuenberger, D., and Mini, O.: Representativeness and seasonality of major ion records derived from NEEM firn cores, The Cryosphere, 8, 1855-1870, 10.5194/tc-8-1855-2014, 2014.

https://doi.org/10.5194/egusphere-2026-3602
Preprint. Discussion started: 9 July 2026

Global Volcanism Program: Volcanoes of the World ((v. 5.2.7; 21 Feb 2025)), Smithsonian Institution [dataset], 10.5479/si.GVP.VOTW5-2024.5.2, 2024.

Gonfiantini, R.: Standards for stable isotope measurements in natural compounds, Nature, 271, 534-536, 10.1038/271534a0, 1978.

Gupta, P., Noone, D., Galewsky, J., Sweeney, C., and Vaughn, B. H.: Demonstration of high-precision continuous measurements of water vapor isotopologues in laboratory and remote field deployments using wavelength-scanned cavity ring-down spectroscopy (WS-CRDS) technology, Rapid Communications in Mass Spectrometry, 23, 2534-2542, 10.1002/rcm.4100, 2009.

Hammer, C. U., Clausen, H. B., and Langway, C. C.: Electrical conductivity method (ECM) stratigraphic dating of the Byrd Station ice core, Antarctica, Annals of Glaciology, 20, 115-120, 10.3189/1994AoG20-1-115-120, 1994.

Hattori, S., Iizuka, Y., Alexander, B., Ishino, S., Fujita, K., Zhai, S., Sherwen, T., Oshima, N., Uemura, R., Yamada, A., Suzuki, N., Matoba, S., Tsuruta, A., Savarino, J., and Yoshida, N.: Isotopic evidence for acidity-driven enhancement of sulfate formation after SO(2) emission control, Sci Adv, 7, 10.1126/sciadv.abd4610, 2021.

Herron, M. M., Herron, S. L., and Langway, C. C.: Climatic signal of ice melt features in southern Greenland, Nature, 293, 389-391, 10.1038/293389a0, 1981.

Hersbach, H., Bell, B., Berrisford, P., Hirahara, S., Horányi, A., Muñoz-Sabater, J., Nicolas, J., Peubey, C., Radu, R., Schepers, D., Simmons, A., Soci, C., Abdalla, S., Abellan, X., Balsamo, G., Bechtold, P., Biavati, G., Bidlot, J., Bonavita, M., De Chiara, G., Dahlgren, P., Dee, D., Diamantakis, M., Dragani, R., Flemming, J., Forbes, R., Fuentes, M., Geer, A., Haimberger, L., Healy, S., Hogan, R. J., Hólm, E., Janisková, M., Keeley, S., Laloyaux, P., Lopez, P., Lupu, C., Radnoti, G., de Rosnay, P., Rozum, I., Vamborg, F., Villaume, S., and Thépaut, J. N.: The ERA5 global reanalysis, Quarterly Journal of the Royal Meteorological Society, 146, 1999-2049, 10.1002/qj.3803, 2020.

Hughes, A. G., Jones, T. R., Vinther, B. M., Gkinis, V., Stevens, C. M., Morris, V., Vaughn, B. H., Holme, C., Markle, B. R., and White, J. W. C.: High-frequency climate variability in the Holocene from a coastal-dome ice core in east-central Greenland, Climate of the Past, 16, 1369-1386, 10.5194/cp-16-1369-2020, 2020.

Iizuka, Y., Matoba, S., Yamasaki, T., Oyabu, I., Kadota, M., and Aoki, T.: Glaciological and meteorological observations at the SE-Dome site, southeastern Greenland Ice Sheet, Bulletin of Glaciological Research, 34, 1-10, 10.5331/bgr.15R03, 2016.

Iizuka, Y., Uemura, R., Fujita, K., Hattori, S., Seki, O., Miyamoto, C., Suzuki, T., Yoshida, N., Motoyama, H., and Matoba, S.: A 60 Year Record of Atmospheric Aerosol Depositions Preserved in a High-Accumulation Dome Ice Core, Southeast Greenland, Journal of Geophysical Research: Atmospheres, 123, 574-589, 10.1002/2017jd026733, 2018.

Iizuka, Y., Matoba, S., Minowa, M., Yamasaki, T., Kawakami, K., Kakugo, A., Miyahara, M., Hashimoto, A., Niwano, M., Tanikawa, T., Fujita, K., and Aoki, T.: Ice Core Drilling and the Related Observations at SE-Dome site, southeastern Greenland Ice Sheet, Bulletin of Glaciological Research, 39, 1-12, 10.5331/bgr.21R01, 2021.

Iizuka, Y., Matsumoto, M., Kawakami, K., Sasage, M., Ishino, S., Hattori, S., Uemura, R., Matsui, H., Fujita, K., Oshima, N., Spolaor, A., Svensson, A., Vinther, B. M., Ohno, H., Seki, O., and Matoba, S.: Acidity-driven gas-particle partitioning of nitrate regulates its transport to Arctic through the industrial era, Nature Communications, 16, 10.1038/s41467-025-59208-0, 2025.

Johnsen, S. J., Clausen, H. B., Dansgaard, W., Fuhrer, K., Gundestrup, N., Hammer, C. U., Iversen, P., Jouzel, J., Stauffer, B., and Steffensen, J. P.: Irregular glacial interstadials recorded in a new Greenland ice core, Nature, 359, 311-313, 10.1038/359311a0, 1992.

Johnsen, S. J., H. B. Clausen, K. M. Cuffey, G. Hoffmann, J. Schwander, and T. Creyts.: Diffusion of stable isotopes in polar firn and ice : the isotope effect in firn diffusion, in: Physics of Ice Core Records, Hokkaido University Press, Sapporo, Hokkaido, Japan, 121-140, 2000.

Jones, T. R., Cuffey, K. M., Roberts, W. H. G., Markle, B. R., Steig, E. J., Stevens, C. M., Valdes, P. J., Fudge, T. J., Sigl, M., Hughes, A. G., Morris, V., Vaughn, B. H., Garland, J., Vinther, B. M., Rozmiarek, K. S., Brashear, C. A., and White, J. W. C.: Seasonal temperatures in West Antarctica during the Holocene, Nature, 613, 292-297, 10.1038/s41586-022-05411-8, 2023.

Kawakami, K., Iizuka, Y., Sasage, M., Matsumoto, M., Saito, T., Hori, A., Ishino, S., Fujita, S., Fujita, K., Takasugi, K., Hatakeyama, T., Hamamoto, S., Watari, A., Esashi, N., Otsuka, M., Uemura, R., Horiuchi, K., Minowa, M., Hattori, S., Aoki, T., Hirabayashi, M., Kawamura, K., and Matoba, S.: SE-Dome II Ice Core Dating With Half-Year Precision:

https://doi.org/10.5194/egusphere-2026-3602
Preprint. Discussion started: 9 July 2026

Increasing Melting Events From 1799 to 2020 in Southeastern Greenland, Journal of Geophysical Research: Atmospheres, 128, 10.1029/2023jd038874, 2023.

Keegan, K. M., Albert, M. R., McConnell, J. R., and Baker, I.: Climate change and forest fires synergistically drive widespread melt events of the Greenland Ice Sheet, Proceedings of the National Academy of Sciences, 111, 7964-7967, 10.1073/pnas.1405397111, 2014.

Laepple, T., Münch, T., Hirsch, N., Shaw, F., and Hörhold, M.: Limitations of ice cores in reconstructing temperature seasonality, Nature, 637, E1-E6, 10.1038/s41586-024-08181-7, 2025.

Lindsey-Clark, J., Grinsted, A., Vandecrux, B., and Schøtt Hvidberg, C.: Greenland Monthly Accumulation Maps (1960–2022): A Statistical Semi-Empirical Bias-Adjustment Model, The Cryosphere, 20, 1463-1495, 10.5194/tc-20-1463-2026, 2026.

Mattingly, K. S., Mote, T. L., Fettweis, X., van As, D., Van Tricht, K., Lhermitte, S., Pettersen, C., and Fausto, R. S.: Strong Summer Atmospheric Rivers Trigger Greenland Ice Sheet Melt through Spatially Varying Surface Energy Balance and Cloud Regimes, Journal of Climate, 33, 6809-6832, 10.1175/jcli-d-19-0835.1, 2020.

Mosley-Thompson, E., McConnell, J. R., Bales, R. C., Li, Z., Lin, P. N., Steffen, K., Thompson, L. G., Edwards, R., and Bathke, D.: Local to regional-scale variability of annual net accumulation on the Greenland ice sheet from PARCA cores, Journal of Geophysical Research: Atmospheres, 106, 33839-33851, 10.1029/2001jd900067, 2001.

Neftel, A., Jacob, P., and Klockow, D.: Measurements of hydrogen peroxide in polar ice samples, Nature, 311, 43-45, 10.1038/311043a0, 1984.

Nghiem, S. V., Hall, D. K., Mote, T. L., Tedesco, M., Albert, M. R., Keegan, K., Shuman, C. A., DiGirolamo, N. E., and Neumann, G.: The extreme melt across the Greenland ice sheet in 2012, Geophys Res Lett, 39, 10.1029/2012gl053611, 2012.

NGRIP-members: High-resolution record of Northern Hemisphere climate extending into the last interglacial period, Nature, 431, 147-151, 10.1038/nature02805, 2004.

Nye, J. F.: Correction Factor for Accumulation Measured by the Thickness of the Annual Layers in an Ice Sheet, Journal of Glaciology, 4, 785-788, 10.3189/s0022143000028367, 1963.

Okazaki, A. and Yoshimura, K.: Development and evaluation of a system of proxy data assimilation for paleoclimate reconstruction, Climate of the Past, 13, 379-393, 10.5194/cp-13-379-2017, 2017.

Ollivier, I., Steen-Larsen, H. C., Dietrich, L. J., Cauquoin, A., Stenni, B., Werner, M., and Landais, A.: Post-depositional Processes Alter the Seasonal and Multi-decadal Water Isotopic Records in Antarctic Snow and Firn, Authorea (preprint), 10.22541/au.175994561.12898624/v1, 2025a.

Ollivier, I., Steen-Larsen, H. C., Stenni, B., Arnaud, L., Casado, M., Cauquoin, A., Dreossi, G., Genthon, C., Minster, B., Picard, G., Werner, M., and Landais, A.: Surface processes and drivers of the snow water stable isotopic composition at Dome C, East Antarctica – a multi-dataset and modelling analysis, The Cryosphere, 19, 173-200, 10.5194/tc-19-173-2025, 2025b.

Paillard, D., Labeyrie, L., and Yiou, P.: Macintosh program performs time-series analysis, EOS Trans. Am. Geophys. Un., 77, 1996.

Pasteris, D. R., McConnell, J. R., Das, S. B., Criscitiello, A. S., Evans, M. J., Maselli, O. J., Sigl, M., and Layman, L.: Seasonally resolved ice core records from West Antarctica indicate a sea ice source of sea-salt aerosol and a biomass burning source of ammonium, Journal of Geophysical Research: Atmospheres, 119, 9168-9182, 10.1002/2013jd020720, 2014.

Plummer, C. T., Curran, M. A. J., van Ommen, T. D., Rasmussen, S. O., Moy, A. D., Vance, T. R., Clausen, H. B., Vinther, B. M., and Mayewski, P. A.: An independently dated 2000-yr volcanic record from Law Dome, East Antarctica, including a new perspective on the dating of the 1450s CE eruption of Kuwae, Vanuatu, Climate of the Past, 8, 1929-1940, 10.5194/cp-8-1929-2012, 2012.

Sakugawa, H., Kaplan, I. R., Tsai, W., and Cohen, Y.: Atmospheric hydrogen peroxide, Environmental Science & Technology, 24, 1452-1462, 10.1021/es00080a002, 2002.

Schneider, A., Zender, C., Loeb, N., and Price, S.: Use of Shallow Ice Core Measurements to Evaluate and Constrain 1980–1990 Global Reanalyses of Ice Sheet Precipitation Rates, Geophys Res Lett, 50, 10.1029/2023gl103943, 2023.

Scholz, D. and Hoffmann, D. L.: StalAge – An algorithm designed for construction of speleothem age models, Quaternary Geochronology, 6, 369-382, 10.1016/j.quageo.2011.02.002, 2011.

https://doi.org/10.5194/egusphere-2026-3602
Preprint. Discussion started: 9 July 2026

Schuenemann, K. C., Cassano, J. J., and Finnis, J.: Synoptic Forcing of Precipitation over Greenland: Climatology for 1961–99, Journal of Hydrometeorology, 10, 60-78, 10.1175/2008jhm1014.1, 2009.

Sigl, M., McConnell, J. R., Layman, L., Maselli, O., McGwire, K., Pasteris, D., Dahl-Jensen, D., Steffensen, J. P., Vinther, B., Edwards, R., Mulvaney, R., and Kipfstuhl, S.: A new bipolar ice core record of volcanism from WAIS Divide and NEEM and implications for climate forcing of the last 2000 years, Journal of Geophysical Research: Atmospheres, 118, 1151-1169, 10.1029/2012jd018603, 2013.

Sigl, M., Winstrup, M., McConnell, J. R., Welten, K. C., Plunkett, G., Ludlow, F., Büntgen, U., Caffee, M., Chellman, N., Dahl-Jensen, D., Fischer, H., Kipfstuhl, S., Kostick, C., Maselli, O. J., Mekhaldi, F., Mulvaney, R., Muscheler, R., Pasteris, D. R., Pilcher, J. R., Salzer, M., Schüpbach, S., Steffensen, J. P., Vinther, B. M., and Woodruff, T. E.: Timing and climate forcing of volcanic eruptions for the past 2,500 years, Nature, 523, 543-549, 10.1038/nature14565, 2015.

Sinnl, G., Winstrup, M., Erhardt, T., Cook, E., Jensen, C. M., Svensson, A., Vinther, B. M., Muscheler, R., and Rasmussen, S. O.: A multi-ice-core, annual-layer-counted Greenland ice-core chronology for the last 3800 years: GICC21, Climate of the Past, 18, 1125-1150, 10.5194/cp-18-1125-2022, 2022.

Steen-Larsen, H. C., Masson-Delmotte, V., Sjolte, J., Johnsen, S. J., Vinther, B. M., Bréon, F. M., Clausen, H. B., Dahl-Jensen, D., Falourd, S., Fettweis, X., Gallée, H., Jouzel, J., Kageyama, M., Lerche, H., Minster, B., Picard, G., Punge, H. J., Risi, C., Salas, D., Schwander, J., Steffen, K., Sveinbjörnsdóttir, A. E., Svensson, A., and White, J.: Understanding the climatic signal in the water stable isotope records from the NEEM shallow firn/ice cores in northwest Greenland, Journal of Geophysical Research, 116, 10.1029/2010jd014311, 2011.

Traufetter, F., Oerter, H., Fischer, H., Weller, R., and Miller, H.: Spatio-temporal variability in volcanic sulphate deposition over the past 2 kyr in snow pits and firn cores from Amundsenisen, Antarctica, Journal of Glaciology, 50, 137-146, 10.3189/172756504781830222, 2004.

Vance, T. R., Abram, N. J., Criscitiello, A. S., Crockart, C. K., DeCampo, A., Favier, V., Gkinis, V., Harlan, M., Jackson, S. L., Kjær, H. A., Long, C. A., Nation, M. K., Plummer, C. T., Segato, D., Spolaor, A., and Vallelonga, P. T.: An annually resolved chronology for the Mount Brown South ice cores, East Antarctica, Climate of the Past, 20, 969-990, 10.5194/cp-20-969-2024, 2024.

Vinther, B. M., Jones, P. D., Briffa, K. R., Clausen, H. B., Andersen, K. K., Dahl-Jensen, D., and Johnsen, S. J.: Climatic signals in multiple highly resolved stable isotope records from Greenland, Quaternary Sci Rev, 29, 522-538, 10.1016/j.quascirev.2009.11.002, 2010.

Vinther, B. M., Clausen, H. B., Johnsen, S. J., Rasmussen, S. O., Andersen, K. K., Buchardt, S. L., Dahl-Jensen, D., Seierstad, I. K., Siggaard-Andersen, M. L., Steffensen, J. P., Svensson, A., Olsen, J., and Heinemeier, J.: A synchronized dating of three Greenland ice cores throughout the Holocene, Journal of Geophysical Research: Atmospheres, 111, 10.1029/2005jd006921, 2006.

Wahl, S., Steen-Larsen, H. C., Hughes, A. G., Dietrich, L. J., Zuhr, A., Behrens, M., Faber, A. K., and Hörhold, M.: Atmosphere-Snow Exchange Explains Surface Snow Isotope Variability, Geophys Res Lett, 49, 10.1029/2022gl099529, 2022.

Winstrup, M., Svensson, A. M., Rasmussen, S. O., Winther, O., Steig, E. J., and Axelrod, A. E.: An automated approach for annual layer counting in ice cores, Climate of the Past, 8, 1881-1895, 10.5194/cp-8-1881-2012, 2012.

Yoshimura, K.: Stable Water Isotopes in Climatology, Meteorology, and Hydrology: A Review, Journal of the Meteorological Society of Japan. Ser. II, 93, 513-533, 10.2151/jmsj.2015-036, 2015.

Yoshimura, K. and Kanamitsu, M.: Dynamical Global Downscaling of Global Reanalysis, Monthly Weather Review, 136, 2983-2998, 10.1175/2008mwr2281.1, 2008.

Yoshimura, K. and Kanamitsu, M.: Incremental Correction for the Dynamical Downscaling of Ensemble Mean Atmospheric Fields, Monthly Weather Review, 141, 3087-3101, 10.1175/mwr-d-12-00271.1, 2013.

Yoshimura, K., Kanamitsu, M., Noone, D., and Oki, T.: Historical isotope simulation using Reanalysis atmospheric data, Journal of Geophysical Research: Atmospheres, 113, 10.1029/2008jd010074, 2008.

Zhang, W., Hou, S., Wu, S.-Y., Pang, H., Sneed, S. B., Korotkikh, E. V., Mayewski, P. A., Jenk, T. M., and Schwikowski, M.: A quantitative method of resolving annual precipitation for the past millennia from Tibetan ice cores, The Cryosphere, 16, 1997-2008, 10.5194/tc-16-1997-2022, 2022.